

1 **pH up-regulation as a potential mechanism for the**  
2 **cold-water coral *Lophelia pertusa* to sustain growth in**  
3 **aragonite undersaturated conditions**

4

5 **M. Wall<sup>1,2</sup>, F. Ragazzola<sup>3,4</sup>, L.C. Foster<sup>3,5</sup>, A. Form<sup>1</sup> and D.N. Schmidt<sup>3</sup>**

6 [1] GEOMAR Helmholtz Centre for Ocean Research Kiel, Germany

7 [2] Alfred Wegener Institute for Polar and Marine Research, Bremerhaven, Germany

8 [3] School of Earth Sciences, University of Bristol, UK

9 [4] now at Institute of Marine Sciences, Portsmouth University, UK

10 [5] now at Marine conservation society, Unit 3, Hereford and Worcester, UK

11

12 Correspondence to: M. Wall (mwall@geomar.de)

13

14

1 **Abstract**

2 Cold-water corals are important habitat formers in deep-water ecosystems and at high  
3 latitudes. Ocean acidification and the resulting change in aragonite saturation are  
4 expected to affect these habitats and impact coral growth. Counter to expectations, the  
5 deep water coral *Lophelia pertusa* has been found to be able to sustain growth even in  
6 undersaturated conditions. However, it is important to know whether such  
7 undersaturation modifies the skeleton and thus its ecosystem functioning. Here we  
8 used Synchrotron X-Ray Tomography and Raman spectroscopy to examine changes  
9 in skeleton morphology and fibre orientation. We combined the morphological  
10 assessment with boron isotope analysis to determine if changes in growth are related  
11 to changes in control of calcification pH. We compared the isotopic composition and  
12 structure formed in their natural environment to material grown in culture at lower pH  
13 conditions. Skeletal morphology is highly variable but shows no distinctive  
14 differences between natural and low pH conditions. Raman investigations found no  
15 difference in macromorphological skeletal arrangement of early mineralization zones  
16 and secondary thickening between the treatments. The  $\delta^{11}\text{B}$  analyses show that *L.*  
17 *pertusa* up-regulates the internal calcifying fluid pH ( $\text{pH}_{\text{cf}}$ ) during calcification  
18 compared to ambient seawater pH and maintain a similar elevated  $\text{pH}_{\text{cf}}$  at increased  
19  $\text{pCO}_2$  conditions. We suggest that as long as the energy is available to sustain the up-  
20 regulation, i.e. individuals are well fed, there is no detrimental to the skeletal  
21 morphology.

22

23

## 1 **1 Introduction**

2 The ocean is absorbing CO<sub>2</sub> from anthropogenic emissions resulting in a drop in  
3 carbonate saturation and ocean pH (Bates et al., 2012). Cold waters take up and store  
4 more CO<sub>2</sub> and thus the high latitudes will be amongst the first to experience  
5 undersaturated conditions (Orr et al., 2005). The response of marine calcifiers to  
6 ocean acidification has been shown to be taxon specific (e.g. Ries et al., 2009, Pörtner  
7 et al., 2014); consequently, understanding the response of important key marine  
8 habitat builders is imperative to estimate potential impacts on their future ecosystem  
9 service. A large number of studies have concentrated on the physiological aspects of  
10 changes in carbonate chemistry (see Pörtner et al., 2014), much less is known about  
11 the impact this has on the skeleton grown by these organisms. While some species  
12 have been shown to continue to grow even under low pH conditions, a weakening of  
13 the ultra-structure can impair ecosystem functionality i.e. its ability to withstand  
14 predators and wave action (Chan et al., 2012; Ragazzola et al., 2012, Melbourne et al.,  
15 2015).

16 Cold-water corals are important habitat builders that offer a range of  
17 microhabitats sustaining high biodiversity and provide nursery grounds for various  
18 species of fish (Fosså et al., 2002; Henry and Roberts, 2007; Roberts et al., 2008). The  
19 maintenance of their structural integrity is essential not just for the species itself but  
20 also for a wide range of species which depend on this habitat. *Lophelia pertusa* is the  
21 most common species of cold-water corals and has a cosmopolitan distribution with a  
22 wide temperature (4-12 °C) and salinity range (35-37 psu) suggesting a relatively  
23 high-tolerance to environmental drivers. The species is typically found in regions with  
24 strong water currents and high productivity (Genin et al., 1986; Mienis et al., 2007).  
25 The modern distribution of cold-water corals appears to be constrained by the  
26 aragonite saturation horizon (the depth below which the waters become  
27 undersaturated with respect to aragonite), with 88.5% of all cold-water coral records  
28 found above the aragonite saturation horizon (Davies and Guinotte, 2011; Guinotte  
29 and Fabry, 2008). Importantly for their future distribution, the aragonite saturation  
30 horizon has shoaled by 80-400m in the North Atlantic since the industrial revolution  
31 (Feely et al., 2004) and model projections suggest a shoaling of up to 2000m by the  
32 end of this century resulting in vast areas of their current habitat being undersaturation  
33 with regards to aragonite (Orr et al., 2005).

1 Despite the strong link between the distribution of cold-water corals and the  
2 aragonite saturation horizon, *Lophelia pertusa* can calcify in undersaturated  
3 conditions (Form and Riebesell, 2012; Hennige et al., 2014; Maier et al., 2009, 2012)  
4 likely facilitated by its ability to increase the internal calcifying fluid pH at the site of  
5 calcification ( $\text{pH}_{\text{cf}}$ ), termed “up-regulation”. Most indications for up-regulation come  
6 from indirect determinations, e.g. measuring the boron isotopic composition ( $\delta^{11}\text{B}$ ) of  
7 bulk skeleton samples of corals (Anagnostou et al., 2012; Holcomb et al., 2014;  
8 McCulloch et al., 2012; Trotter et al., 2011). Measurement of the  $\text{pH}_{\text{cf}}$  at the site of  
9 calcifications in several corals confirmed an ability of the organism to influence the  
10 internal  $\text{pH}_{\text{cf}}$  with a range of physiological processes (Al-Horani, 2003; Ries, 2011;  
11 Venn et al., 2013). The skeletal  $\delta^{11}\text{B}$  was observed to decrease with lower saturation  
12 state and pH of seawater (in total scale:  $\text{pH}_{\text{T}}$ ), suggesting a relative lowering of the  
13 internal  $\text{pH}_{\text{cf}}$  in response to external pH decrease. At low seawater  $\text{pH}_{\text{T}}$ , internal  $\text{pH}_{\text{cf}}$   
14 is still significantly higher than seawater  $\text{pH}_{\text{T}}$  (up-regulation intensity, where  $\Delta\text{pH} =$   
15  $\text{pH}_{\text{cf}} - \text{pH}_{\text{T}}$  (Anagnostou et al., 2012; McCulloch et al., 2012; Trotter et al., 2011)),  
16 but does not reach internal  $\text{pH}_{\text{cf}}$  levels observed under control conditions (Holcomb et  
17 al., 2014; Trotter et al., 2011).

18 This up-regulation ability has several implications: Firstly, the potential to  
19 moderate the impact of projected future saturation state depends on the strength and  
20 efficiency of this mechanism (less efficient up-regulating species may be more  
21 adversely affected). Secondly, such differences in efficiencies will affect the  
22 reliability of  $\delta^{11}\text{B}$  as pH proxy when applied to paleo-climate reconstruction. Thirdly,  
23 the establishment of a pH gradient between external seawater and internal site of  
24 calcification requires energy reallocation (Al-Horani et al., 2003; Chalker and Taylor,  
25 1975) and altered energetic demands may affect skeletal structure and strength.

26 In order to understand the interaction of biomineralisation response, we analysed  
27 *L. pertusa* skeletons grown under natural control (Sula Reef  $\text{pCO}_2 = 405 \mu\text{atm}$ ) and  
28 elevated  $\text{CO}_2$  conditions (CRSIII  $\text{pCO}_2 = 982 \mu\text{atm}$ ). We uniquely combined Raman  
29 spectroscopy, Secondary Ionisation Mass Spectrometry (SIMS) and Synchrotron X-  
30 ray Tomographic Microscopy (SXRTM) to examine whether ocean acidification  
31 causes any change in skeletal morphology of *L. pertusa*, such as thickness and growth  
32 patterns, or in the biomineralisation processes. SIMS  $\delta^{11}\text{B}$  transects are compared  
33 between the high  $\text{pCO}_2$  (CRSIII) treatment and the natural conditions (Sula Reef).

1 The  $\delta^{11}\text{B}$  are converted to  $\text{pH}_{\text{cf}}$  to examine potential physiological adjustments in  
2 coral biomineralisation under anticipated future ocean conditions of lower  $\text{pH}_{\text{T}}$ .

## 3 4 **2 Material and Methods**

### 5 **2.1 Specimens**

6 The *Lophelia pertusa* specimens grown in an experimental set-up at GEOMAR,  
7 Germany (see Form & Riebesell (2012) for full details about the experimental set-up).  
8 In brief, the live branches of *L. pertusa* were collected with minimal invasion using  
9 the manned submersible JAGO at the central part of the Sula Reef complex (64°06'N,  
10 8°05'E) off the Norwegian coast in 2008. The samples were transferred to Kiel and  
11 after a 3-month acclimatisation period they were stained using Alizarin Red S  
12 (Standard Fluka: Sigma-Aldrich, Steinheim, Germany, with a concentration of 5 mg/L  
13 for an incubation period of eight days to mark the start of the experiment). The corals  
14 were kept at a constant temperature (7.5 °C) and salinity (34.5 psu) similar to the  
15 conditions at the Sula Reef. After staining, the corals were transferred to the treatment  
16 tanks and the  $\text{pCO}_2$  was over two weeks gradually adjusted to the treatment  
17 conditions which are summarized in Table 1. The specimens were cultured for 6  
18 month in all treatments. SIMS  $\delta^{11}\text{B}$  transects and Raman are compared between the  
19 high  $\text{pCO}_2$  (CRSIII) treatment and the natural conditions (Sula Reef), while for  
20 SRXTM and wall thickness measurements individuals from all treatments were used  
21 (CRSI  $\text{pCO}_2 = 605 \mu\text{atm}$ , CRSII  $\text{pCO}_2 = 778 \mu\text{atm}$  and CRSIII  $\text{pCO}_2 = 982 \mu\text{atm}$ ).

22 Cold-water corals show isotopic (including  $\delta^{11}\text{B}$ ) and elemental heterogeneities  
23 within the early mineralizing skeleton (including EMZ like structure in the theca wall,  
24 e.g. Adkins et al., 2003; Blamart et al., 2007). To overcome this heterogeneity, studies  
25 using cold-water corals to trace seawater  $\text{pH}_{\text{T}}$  limit the sampling to the outer thecal  
26 wall and integrate large skeletal areas (e.g. McCulloch et al. 2012, Anagnostou et al.  
27 2012). Main growth occurs at the polyp tip, where the theca wall is very thin and  
28 predominately formed by primary skeleton. This area is normally avoided in boron  
29 studies as it is calcified under a different mechanisms then the secondary theca  
30 thickening.

31 Cold-water corals grow slowly which makes is impossible for us to follow this  
32 approach. It would also limit our analysis to a part of the skeleton and not allow the  
33 more holistic look at the growth we would like to achieve. To evaluate the  $\delta^{11}\text{B}$

1 change with changing seawater conditions and to be able to link this directly to  
2 structural material analysis, a high-spatial resolution technique was applied to  
3 material that was grown during the culturing period. To separate the growth of the  
4 skeleton during natural and treatment conditions, we traced the Alizarin staining line.  
5 In the theca wall where growth is slower Alizarin was incorporated in traces and we  
6 used Raman spectroscopy to determine the start of the experiments.

7 For Raman and SIMS analyses, specimens cultured in the high treatment ( $982 \pm$   
8  $146 \mu\text{atm}$ ) were compared to branches/skeletal regions grown naturally in the field.  
9 The specimens were cut transversal (at different heights along the corallite) and  
10 longitudinal. From the high  $p\text{CO}_2$  treatment (CRSIII) one polyp was cut above and  
11 below the Alizarin stain (Fig. 1b) and another polyp was cut transversally through the  
12 thecal wall. The sample preparations allow a comparison of skeleton grown naturally  
13 *in situ* to pre-study conditions and during the culturing time prior to the staining as  
14 well as the treatment conditions after staining.

## 16 **2.2 Raman mapping**

17 Raman mapping was done using a WITec alpha 300 R (WITec GmbH, Germany)  
18 Confocal Raman Microscope equipped with an ultra-high throughput spectrometer  
19 (UHTS 300, WITec, Germany) and an EMCCD camera (grating of  $600 \text{ grooves mm}^{-1}$   
20  $^1$ , blazed at  $500 \text{ nm}$  and centred at  $2400 \text{ cm}^{-1}$ ). Laser excitation wavelength of  $488 \text{ nm}$   
21 was used. Raman maps were derived using a Nikon 20x (numeric aperture (NA) =  
22  $0.4$ ) objective for large area scans and a Nikon 100x (NA =  $0.9$ ) for small high-  
23 resolution area scans. The spectra during mapping were recorded with an integration  
24 time of  $35 \text{ ms}$  and a step size of  $1 \mu\text{m}$  (large area scans) and  $10 \text{ ms}$  and  $0.5 \mu\text{m}$  for  
25 small area scans. The symmetric stretch of the carbonate ( $1085 \text{ cm}^{-1}$ ) provides  
26 information on the crystal orientations and was used to map the skeletal growth  
27 patterns and arrangement. Fluorescence intensity distribution (in the spectral range  
28 between  $2400\text{-}2700 \text{ cm}^{-1}$ ) was used as a proxy to map organic matrix distribution  
29 within biogenic minerals (Wall and Nehrke, 2012) as well as to map the location of  
30 the staining line where it was not visible in microscopic images. All Raman spectral  
31 data sets were processed using the WITec Project software (version 2.04, WITec  
32 GmbH, Germany).

33 Transversal sections of *L. pertusa* calices show differences in skeletal densities  
34 (Fig. 1a) visible as differences in opaqueness of the skeleton. This criterion is often

1 used to determine growth rings and to identify nucleation zones, which are  
 2 characterized by distinct elemental ratios and isotopic signatures (Mortensen and  
 3 Rapp, 1998; Wainright, 1964) compared to the bulk thecal skeleton (Adkins et al.,  
 4 2003; Blamart et al., 2007; Cohen et al., 2006). Confocal Raman maps of the  
 5 aragonite symmetric stretch intensity (the intensity of the main carbonate peak) allows  
 6 similarly to distinguish the different skeletal regions (for detailed information see  
 7 Wall and Nehrke, 2012). Here, skeletal regions were divided into a primary skeleton  
 8 around the central corallite line (composed of EMZ) and paralleled layered fibre  
 9 growth, giving the corallites their shape and size. A secondary thickening is  
 10 subsequently responsible for the addition of skeletal mass to the corallite theca (Fig.  
 11 1e). The growth patterns within primary and secondary skeleton are compared  
 12 between natural conditions and the treatments and used to relate the boron isotopic  
 13 signature to the different growth stages.

14

### 15 **2.3 $\delta^{11}\text{B}$ with SIMS**

16 Boron isotopes in marine biogenic carbonates are a pH-proxy, which varies  
 17 systematically with seawater pH (e.g. Hemming & Hanson, 1992; Rae et al., 2011).  
 18 The value recorded depends on a strong biological control (“vital effect”) and reflects  
 19 internal calcifying fluid  $\text{pH}_{\text{cf}}$  (Hönisch et al., 2004; Holcomb et al., 2014; McCulloch  
 20 et al., 2012). The following equation converts  $\delta^{11}\text{B}$  into pH (or  $\text{pH}_{\text{cf}}$ ):

$$21 \quad \text{pH} = \text{pK}^*_B - \log\left[\frac{\delta^{11}B_{\text{sw}} - \delta^{11}B_C}{\alpha_B * \delta^{11}B_C - \delta^{11}B_{\text{sw}} + 1000 * (\alpha_B - 1)}\right] \quad (1)$$

22  $\text{pK}^*_B$  = dissociation constant of boric acid (Dickson, 1990). The theoretical  $\delta^{11}\text{B}$   
 23 for the sample location can be calculated using  $\text{pK}^*_B = 8.795$  for the natural *in situ*  
 24 grown skeletal and  $\text{pK}^*_B = 8.814$  for the treatment specimen.  $\text{pK}^*_B$  values were  
 25 calculated from seacarb using the software package R (Lavigne and Gattuso, 2010).

26  $\alpha_B$  = isotopic fractionation factor in seawater at 25°C is  $1.0272 \pm 0.0006$  (Klochko  
 27 et al., 2006).

28  $\delta^{11}B_{\text{sw}}$  = boron isotope composition of seawater is 39.61 ‰ (Foster et al., 2010)

29  $\delta^{11}B_C$  = measured  $\delta^{11}\text{B}$  of the studied coral specimen

30

31 For SIMS measurements we used the Cameca-ims-f4 and the Cameca-ims-1270  
 32 at the EMMAC facility, University of Edinburgh with the following measuring

1 procedure: The sections were gold-coated and analysed with a  $^{16}\text{O}_2^-$  primary beam.  
2 For the f4 the primary beam energy was 15 keV and a beam current between 10 and  
3 40 nA to produce positive secondary ions of 10B+ and 11B+ and for the 1270 a  
4 primary beam energy of 12.2 keV and secondary ion energy of 10keV resulting in a  
5 net primary impact energy of 22 keV. The secondary ions were analysed with an  
6 energy window of 52 eV, a 150  $\mu\text{m}$  image field using 450  $\mu\text{m}$  contrast and 1800  $\mu\text{m}$   
7 field apertures. Surface contamination was minimised using a 30 second pre-sputter,  
8 Köhler illumination with a field aperture limiting ions to the central area of the sputter  
9 pit. The isotope ratio was measured for 200 cycles for the f4 and 60 cycles for the  
10 1270 per spot analysis, each cycle consisting of 5 and 3 s integrations of 10B+ and  
11 11B+ respectively. The beam diameter at the end of the analysis was  $\sim 25$  by  $40$   $\mu\text{m}$ .  
12 For details see Kasemann et al. (2009). Analyses followed line-transects and single  
13 spots were spaced  $\sim 30$ - $50$   $\mu\text{m}$  apart (depending on the sampling location). A  
14 minimum of 10 spot analyses of the internal standard M93 coral bulk standard  
15 (Kasemann et al., 2009) ( $24.8 \pm 0.4$  ‰ (2SD)) was run each day of analyses on both  
16 instruments, with an average of  $3.79 \pm 0.44$  ‰ (1SE) and used to normalize sample  
17  $^{11}\text{B}/^{10}\text{B}$  values.

18 We analysed three colonies from Sula reef to assess the variability within the  
19 population. We tested how representative our cross sections are by analysing two  
20 sections from the same corallite. We also tested reproducibility of our results by  
21 comparing two corallites from the same coral colony and then compared growth prior  
22 to staining with material grown in culture (for schematic representation see  
23 supplementary material Fig. S1).

24

## 25 **2.4 Synchrotron analyses and wall thickness changes**

26 Synchrotron-based X-ray Tomographic Microscopy were performed at the  
27 TOMCAT beamline at the Swiss Light Source, Paul Scherrer Institut, Villigen,  
28 Switzerland (Stampanoni et al., 2006). One specimen from each of the  $\text{CO}_2$  levels was  
29 scanned (CRSI-CRSIII:  $604 \pm 105$   $\mu\text{atm}$ ,  $778 \pm 112$   $\mu\text{atm}$  and  $982 \pm 146$   $\mu\text{atm}$ ). For  
30 each tomographic scan, 377 projections over 180 degrees were acquired at energy of  
31 28 keV with UPLAPO 2x objective (field view of  $7.5 \times 7.5$   $\text{mm}^2$ ; pixel size  $3.7 \times 3.7$   
32  $\text{mm}^2$ ). The exposure time was 250 ms. Further processing was done using Avizo to  
33 produce 3D isosurface model and measure sample thickness above and below  
34 Alizarin stain lime (Fig. 2b) by cross-referencing to the sample. In addition,

1 longitudinal cuts of *Lophelia pertusa* polyps (n = 5-7, per treatment) grown at the  
2 distal ends of the colonies were analyzed with microscope to measure wall thickness  
3 below and above the staining line. The thickness ratio of below and above staining  
4 line was calculated and compared between treatments. Polyp diameter is not  
5 correlated to linear extension of a polyp (Fig. S2) nor the location (Form, pers  
6 communication).

7

### 8 **3 Results**

9 The main growing edge outlined by the Alizarin staining lines marks the border  
10 to the experimentally precipitated distal skeleton (Fig. 2). In microscopic images, the  
11 staining line is only visible at the main growing edge (Fig. 2b), whereas in Raman  
12 fluorescence maps the outer skeletal surface before the start of the experiment can be  
13 traced over the entire colony (Fig. 2,3). The Raman maps clearly display the  
14 orientation of the skeletal fibres and the location of the early mineralization zone  
15 (EMZ: Cuif and Dauphin, 2005, or rapid accretion front, RAF Stolarski, 2003) and  
16 were used to compare skeletal formation before and during experimental conditions  
17 (Fig. 2c,d). At the macromorphological level, i.e. the arrangement of the main  
18 skeleton entities (EMZ and fibres), no notable difference between the natural and high  
19  $p\text{CO}_2$  sample can be detected (Fig. 3c,d, 5,6b).

20 Skeletal tomography reveals a large degree of morphological variability within  
21 the *L. pertusa* skeleton. Both, the thickness of the outer wall and septa vary strongly  
22 as do the shape and length of the septa (Fig. 7). In addition, the vertical extension of  
23 newly grown material (after staining) was not even (Fig. 7). To enable a direct  
24 comparison between the natural material and that grown at high  $\text{CO}_2$ , sections were  
25 taken directly above and below the Alizarin stain (Fig. 7b). These sections show that  
26 there is no change in structure for three different  $p\text{CO}_2$  treatments (Fig. 7 c-h) which  
27 was confirmed by measurements on longitudinal polyp sections (supplementary  
28 material Fig. S3). Overall thickness is slightly higher below the staining line than  
29 above (thickness ratio below/above of  $1.10 \pm 0.07$ ) and range from  $0.82 (\pm 0.04)$ ,  $1.14$   
30  $(\pm 0.09)$  to  $1.32 (\pm 0.16)$  for the CRSII, CRSI and CRSII, respectively (see  
31 supplementary material Fig. S3).

32 All the samples and transects analysed for boron isotopes are summarized in  
33 Table 2. Repeated cross sections of the same corallites are reproducible (same colony  
34 and same polyp  $\delta^{11}\text{B}$  mean  $\pm$  SE:  $26.41\text{‰} \pm 0.83$  vs  $26.08\text{‰} \pm 0.61$  and  $27.62\text{‰} \pm$

1 1.09 vs 27.55‰ ± 0.57) as were transects comparing two coral polyps from the same  
2 coral colony (27.96‰ ± 0.48 vs 27.62‰ ± 1.09). Hence, we observed consistent  
3 values within the population grown in their natural environment within error.

4 All transects show heterogeneity in  $\delta^{11}\text{B}$  varying from ~19.8-32.2 ‰, in  
5 particular when old branches with secondary thickening were analysed (Fig. 4, 6,  
6 supplementary material Fig. S4). The variability of  $\delta^{11}\text{B}$  in *L. pertusa* spans approx.  
7 14 ‰ and reveals lower values within the primary skeleton around the EMZ 22.48 ±  
8 1.58 ‰ (mean ± SD, see electronic supplementary material Table S1) and an increase  
9 towards the outer skeletal rims (Fig. 4,6, see electronic supplementary material Fig.  
10 S4,S5). The secondary thickening is characterized by a higher  $\delta^{11}\text{B}$  of 26.97 ± 4.73 ‰  
11 compared to the primary material and slightly reduced values at opaque nucleation  
12 sites (Fig. 6, see electronic supplementary material Fig. S4).

13 Material that was deposited along the same skeletal region has the same  $\delta^{11}\text{B}$   
14 (shown by repeated transects on several polyps; Fig. 4,5). Transects on different  
15 polyps with similar diameter of the same colony show the same  $\delta^{11}\text{B}$  (transect 3,4,  
16 Table 2). The secondary thickening has the same  $\delta^{11}\text{B}$  independent of whether it was  
17 precipitated during natural or the high  $p\text{CO}_2$  condition (26.97 ± 4.73 ‰ and 27.8 ±  
18 1.94 ‰, respectively; Fig. 3c) corresponding to a  $\text{pH}_{\text{cf}}$  of 8.94 ± 0.15 or 8.95 ± 0.13,  
19 respectively. The sample grown only under high  $p\text{CO}_2$  has slightly higher average  
20  $\delta^{11}\text{B}$  (24.52 ± 1.21 ‰) within the primary skeleton (Fig. 6) compared to primary  
21 skeleton precipitated under natural conditions. During the formation of the primary  
22 skeleton the calculated internal calcifying fluid  $\text{pH}_{\text{cf}}$  is lower than during secondary  
23 thickening (8.58 ± 0.11 vs. 9.01 ± 0.15). The primary skeleton formed during high  
24  $p\text{CO}_2$  conditions reveals a stronger internal pH up-regulation (8.74 ± 0.08) but still  
25 lower values than what was measured within the secondary thickening during high  
26  $\text{CO}_2$  conditions (8.95 ± 0.13).

#### 28 4 Discussion

30 *Lophelia pertusa* has been shown to grow in undersaturated conditions. The  
31 amount of aragonite deposited under higher  $\text{CO}_2$  was at least equivalent to that  
32 deposited under natural conditions in agreement with findings in other studies  
33 showing sustained calcification using different analytical approaches (Form and

1 Riebesell, 2012; Hennige et al., 2014; Maier et al., 2012). As *L. pertusa* grows by  
2 both vertical extension and by thickening, measurements by buoyant weight though  
3 do not provide information on whether the morphology is affected, i.e. does the  
4 skeleton thicken or thin during low saturation or remain unchanged.

5 Tomographic analyses showed that the morphology of *Lophelia* skeletons is  
6 highly variable and does not change under high CO<sub>2</sub> even in undersaturated waters.  
7 We observed no change in the internal structure, in contrast other calcifying  
8 organisms, which show wall deformation in tube worms or coralline algae (Chan et  
9 al., 2012; Ragazzola et al., 2012). Arrangement and size of the primary skeleton, the  
10 template of size and shape of the corallite, do not change between treatments. The  
11 succession of growth bands is maintained and layers are formed even at  
12 undersaturated conditions. This finding corroborates a strong biological control on  
13 coral biomineralisation. The only exception were less distinct organic layers, which  
14 might represent an impact on biomineralisation in response to ocean acidification. The  
15 wider implications of a changed skeletal organic matrix need to be investigated  
16 further to understand its full implications.

17 A strong biological control on the biomineralisation should also be expressed in  
18 its chemical composition, especially the boron isotope compositions (McCulloch et  
19 al., 2012, Hönisch et al., 2004). As deep-water corals grown in relatively stable  
20 environmental conditions, the high-resolution spatial isotopic and elemental  
21 heterogeneities suggest a biotic control that changes during growth. The isotopic  
22 heterogeneity is associated with specific skeletal regions (Blamart et al., 2007) and is  
23 also observed in other isotopes, e.g.  $\delta^{18}\text{O}$  (e.g. Rollion-Bard et al., 2010) and  
24 elemental ratios, e.g. Mg/Ca (e.g. Cohen et al., 2006, Krief et al., 2010). The Early  
25 Mineralization Zone (EMZ) is characterised with relatively low  $\delta^{11}\text{B}$  compared to  
26 adjacent fibrous aragonite with a higher  $\delta^{11}\text{B}$  and increases towards the outer wall.  
27 The EMZ is also known to have systematically lighter C and O isotopic composition  
28 by ~4-5 ‰ and ~8-10 ‰ respectively, compared to the fibrous aragonite part (Juillet-  
29 Leclerc et al., 2009; Rollion-Bard et al., 2010). Differences in C and O isotopes are  
30 suggested to be related to a faster growth of the EMZ suggesting that different skeletal  
31 regions are grown under different control or potentially even precipitation  
32 mechanisms. While the degree of heterogeneity with respect to boron isotopes in our  
33 samples is roughly equivalent to that of Blamart et al. (2007), the absolute values are

1 offset by ~10-14 ‰. In their study the  $\delta^{11}\text{B}$  translates to a maximum  $\text{pH}_{\text{cf}}$  of  
2 approximately 10.2, while our data suggest values around 8.8 to 8.9 and agree with  
3 the bulk measurements of *L. pertusa* (McCulloch et al., 2012) and direct  
4 measurements of pH of calcifying fluids in symbiotic Scleractinian corals (Al-Horani  
5 et al., 2003) which determined values of 9.28 at light (additionally elevated by  
6 symbiont activity) and 8.13 at dark with seawater values of 8.2.

7 The use of  $\delta^{11}\text{B}$  as  $\text{pH}_{\text{T}}$  proxy is based on exclusive borate incorporation. Rollion-  
8 Bard et al. (2011), by re-analysing samples from Blamart et al. (2007), suggested that  
9 both borate and boric acid are incorporated in the skeleton of *Lophelia pertusa*. In  
10 their study they observed NMR differences in skeletal boron coordination, which was  
11 used as indicator for boric acid incorporation. Considering the fraction of boric acid  
12 incorporation, they obtained  $\text{pH}_{\text{cf}}$  values similar to values obtained in other  
13 (McCulloch et al., 2012) and this study. In addition, they suggested that the EMZ  
14 incorporated a higher proportion of boric acid. In our data, we did not test whether  
15 boric acid incorporation plays a role. Our  $\delta^{11}\text{B}$  to pH calculations though do not need  
16 any changes in incorporation to yield values which are comparable to bulk  
17 measurements (McCulloch et al., 2012). Applying their model to our data using  $\delta^{11}\text{B}$   
18 signature of the EMZ, the same individual would incorporate very different  
19 proportions of boric acid which is not likely given the broad range of literature on  
20 boron in corals in general. Therefore, we question this variable boric acid  
21 incorporation hypothesis.

22 Our interpretations are based on the internal  $\text{pH}_{\text{cf}}$  regulation calcification model  
23 (McCulloch et al., 2012) which assumes that the  $\text{pH}_{\text{cf}}$  is offset from seawater  $\text{pH}_{\text{T}}$ .  
24 McCulloch et al. (2012) reported a decrease in  $\delta^{11}\text{B}$  with decreasing  $\text{pH}_{\text{T}}$  in several  
25 cold-water coral species including *L. pertusa*. They suggested that biological  $\text{pH}_{\text{cf}}$  up-  
26 regulation determines the calcification response as described also for tropical corals  
27 (Holcomb et al., 2014). In contrast, we find similar growth rates between  $\text{pCO}_2$   
28 treatments (Form and Riebesell, 2012) and similar  $\delta^{11}\text{B}$  values (within a 0.3 pH unit  
29 error) which questions a decreasing internal  $\text{pH}_{\text{cf}}$  (Anagnostou et al., 2012;  
30 McCulloch et al., 2012).

31 If our interpretation of maintenance of internal  $\text{pH}_{\text{cf}}$  within the secondary skeleton  
32 is correct it suggests that pH regulation can be decoupled from external seawater  $\text{pH}_{\text{T}}$   
33 and is a mechanism to explain the cold-water coral resilience. There are a number of

1 parameters underreported in most acidification studies which might explain the  
2 difference in our findings. For example it has been suggested for a range of organisms  
3 that given a sufficient food supply, calcification can be maintained despite low  
4 saturation state (Schoepf et al., 2013; Thomsen et al., 2013). One possible explanation  
5 why we did not see a difference between treatments and the natural environment  
6 could be that food was provided in higher amounts than other studies on *Lophelia* and  
7 hence additional energy might have been available to support calcification. If this is  
8 the case than limited food availability might have a strong impact on the ability to  
9 regular the internal pH and *Lophelia* growth (Rodolfo-Metalpa et al. 2015).  
10 Respiration rates of *Lophelia* were observed to decline (Hennige et al., 2014, Form  
11 and Riebesell 2012) or unchanged (Maier et al., 2013) under elevated  $p\text{CO}_2$   
12 suggesting that other energy sources, e.g. lipids, were used to maintain growth  
13 assuming other metabolic processes remained constant. Unfortunately, our growth  
14 experiments did not monitor whether reduced respiration changes the availability of  
15 energy reserves or tissue biomass between the treatments and presents an important  
16 scope for a new study of the physiological consequences of  $\text{pH}_{\text{cf}}$  up-regulation and  
17 associated energy requirements.

18 We have found indications of changes in the organic matrix (OM). These less  
19 distinct OM bands could be an important step in biomineralisation compromised  
20 under ocean acidification. In a tropical coral, OM production has been found to be  
21 affected by both up and down regulation of certain OM protein encoding genes (Moya  
22 et al., 2012), which might result in changes in the quality of the OM. The layered  
23 growth of biogenic organisms is a prominent feature (Cuif and Dauphin, 2005) and  
24 suggests a strong biological control of growth. Thus, a less clear banding could  
25 indicate that OM formation is compromised. However, further studies are necessary  
26 to better characterize the role, function and importance of skeletal organic layers.

27 In conclusion, the lack of sensitivity of *L. pertusa* to changes in  $p\text{CO}_2$  in growth,  
28 mineralogy and boron isotopes corroborates their strong biological control over  
29 biomineralisation that is not easily disturbed under elevated  $p\text{CO}_2$  conditions. Our  
30 results raise a number of question: (1) can energy be reallocated to up-regulate the  
31 internal  $\text{pH}_{\text{cf}}$  to a suitable level which would complicate the applicability of *Lophelia*  
32 *skeletons*  $\delta^{11}\text{B}$  record as a paleo-pH proxy given the small ranges of pH difference  
33 studies often aim to resolve and (2) the role of OM production and quality need to be

1 considered to improve our understanding of cold-water coral biomineralisation and  
2 their response to acidification.

3

#### 4 **Author contribution statement**

5 AF provided the specimens from the culturing experiment. MW, LCF, FR & DNS  
6 collected the data. MW, LCF, DNS, FR and AF analyzed the data. MW, LCF, FR  
7 wrote the paper, and all authors (MW, LCF, FR, DNS & AF) contributed to the final  
8 text and figures.

9

#### 10 **Acknowledgments**

11 This study is a contribution to the BIOACID joint project, funded by the German  
12 Ministry of Research and Technology and EPOCA. The tomographic analyses were  
13 performed on the TOMCAT beamline at the Swiss Light Source (SLS), Paul Scherrer  
14 Institut, Villigen, Switzerland (SLS grant Agreement Number no. 20110822). The  
15 staff at EMMAC are thanked for their assistance with analyses, supported by a small  
16 research grant from the Royal Society. We are grateful to Federica Marone at the  
17 Swiss Light Source whose outstanding efforts have made these experiments possible.  
18 MW has received funding from the FP7-PEOPLE-2007-1-1-ITN Marie Curie Action:  
19 CalMarO (Calcification by Marine Organisms, Grant number: 215157) and BIOACID  
20 II (Grant number: FKZ 03F0655A). LCF acknowledges support from the Holmes  
21 Fellowship and NERC grant NE/F017383/1. FR is supported by Leverhulme  
22 Research Grant and DNS via a URF from the Royal Society.

23

#### 24 **References**

25 Adkins, J. F., Boyle, E. A., Curry, W. B. and Lutringer, A.: Stable isotopes in  
26 deep-sea corals and a new mechanism for "vital effects," *Geochemica*  
27 *Cosmochem. Acta*, 67(6), 1129–1143, doi:10.1016/S0016-7037(02)01203-6,  
28 2003.

29 Al-Horani, F. A., Al-Moghrabi, S. M. and de Beer, D.: The mechanism of  
30 calcification and its relation to photosynthesis and respiration in the scleractinian  
31 coral *Galaxea fascicularis*, *Mar. Biol.*, 142, 419–426, doi:10.1007/s00227-002-  
32 0981-8, 2003.

33 Anagnostou, E., Huang, K., You, C., Sikes, E. L. and Sherrell, R. M.: Evaluation of  
34 boron isotope ratio as a pH proxy in the deep sea coral *Desmophyllum dianthus* :

1 Evidence of physiological pH adjustment, *Earth Planet. Sci. Lett.*, 349-350, 251–  
2 260, doi:10.1016/j.epsl.2012.07.006, 2012.

3 Bates, N. R., Best, M. H. P., Neely, K., Garley, R., Dickson, a. G. and Johnson, R.  
4 J.: Detecting anthropogenic carbon dioxide uptake and ocean acidification in the  
5 North Atlantic Ocean, *Biogeosciences*, 9(7), 2509–2522, doi:10.5194/bg-9-2509-  
6 2012, 2012.

7 Blamart, D., Rollion-Bard, C., Meibom, A., Cuif, J.-P., Juillet-Leclerc, A. and  
8 Dauphin, Y.: Correlation of boron isotopic composition with ultrastructure in the  
9 deep-sea coral *Lophelia pertusa*: Implications for biomineralization and paleo-pH,  
10 *Geochemistry, Geophys. Geosystems*, 8(12), 1–11, doi:10.1029/2007GC001686,  
11 2007.

12 Chalker, B. E. and Taylor, D. L.: Light-enhanced calcification, and the role of  
13 oxidative phosphorylation in calcification of the coral *Acropora cervicornis*, *Proc.*  
14 *Biol. Sci.*, 190, 323–331, 1975.

15 Chan, V. B. S., Li, C., Lane, A. C., Wang, Y., Lu, X., Shih, K., Zhang, T. and  
16 Thiyagarajan, V.: CO<sub>2</sub>-driven ocean acidification alters and weakens integrity of  
17 the calcareous tubes produced by the serpulid tubeworm, *Hydroides elegans.*,  
18 *PLoS One*, 7(8), e42718, doi:10.1371/journal.pone.0042718, 2012.

19 Cohen, A. L., Gaetani, G. a., Lundälv, T., Corliss, B. H. and George, R. Y.:  
20 Compositional variability in a cold-water scleractinian, *Lophelia pertusa*: New  
21 insights into “vital effects,” *Geochemistry, Geophys. Geosystems*, 7(12), n/a–n/a,  
22 doi:10.1029/2006GC001354, 2006.

23 Cuif, J.-P. and Dauphin, Y.: The two-step mode of growth in the scleractinian  
24 coral skeletons from the micrometre to the overall scale, *J. Struct. Biol.*, 150,  
25 319–331, doi:10.1016/j.jsb.2005.03.004, 2005.

26 Davies, A. J. and Guinotte, J. M.: Global habitat suitability for framework-forming  
27 cold-water corals., *PLoS One*, 6(4), e18483, doi:10.1371/journal.pone.0018483,  
28 2011.

29 Farmer, J.R., Hönisch, B., Robinson, L.F., Hill, T.M., 2015. Effects of seawater-pH  
30 and biomineralization on the boron isotopic composition of deep-sea bamboo  
31 corals. *Geochimica et Cosmochimica Acta* 155, 86-106.

32 Feely, R. a, Sabine, C. L., Lee, K., Berelson, W., Kleypas, J., Fabry, V. J. and  
33 Millero, F. J.: Impact of anthropogenic CO<sub>2</sub> on the CaCO<sub>3</sub> system in the oceans.,  
34 *Science*, 305(5682), 362–6, doi:10.1126/science.1097329, 2004.

35 Form, A. U. and Riebesell, U.: Acclimation to ocean acidification during long-term  
36 CO<sub>2</sub> exposure in the cold-water coral *Lophelia pertusa*, *Glob. Chang. Biol.*, 18(3),  
37 843–853, doi:10.1111/j.1365-2486.2011.02583.x, 2012.

1 Fosså, J. H., Mortensen, P. B. and Furevik, D. M.: The deep-water coral *Lophelia*  
2 *pertusa* in Norwegian waters: distribution and fishery impacts, *Hydrobiologia*,  
3 471, 1–12, 2002.

4 Foster, G. L., Pogge von Strandmann, P. a. E. and Rae, J. W. B.: Boron and  
5 magnesium isotopic composition of seawater, *Geochemistry, Geophys.*  
6 *Geosystems*, 11(8), n/a–n/a, doi:10.1029/2010GC003201, 2010.

7 Genin, A., Dayton, P. K., Lonsdale, P. F. and Spiess, F. N.: Corals on seamount  
8 peaks provide evidence of current acceleration over deep-sea topography,  
9 *Nature*, 322, 59–61, 1986.

10 Guinotte, J. M. and Fabry, V. J.: Ocean acidification and its potential effects on  
11 marine ecosystems., *Ann. N. Y. Acad. Sci.*, 1134, 320–42,  
12 doi:10.1196/annals.1439.013, 2008.

13 Hemming, N.G., Hanson, G.N., 1992. Boron isotopic composition and  
14 concentration in modern marine carbonates. *Geochimica Cosmochimica Acta* 56,  
15 537-543.

16 Hennige, S. J., Wicks, L. C., Kamenos, N. a., Bakker, D. C. E., Findlay, H. S.,  
17 Dumousseaud, C. and Roberts, J. M.: Short-term metabolic and growth responses  
18 of the cold-water coral *Lophelia pertusa* to ocean acidification, *Deep Sea Res. Part*  
19 *II Top. Stud. Oceanogr.*, 99, 27–35, doi:10.1016/j.dsr2.2013.07.005, 2014.

20 Henry, L.-A. and Roberts, J. M.: Biodiversity and ecological composition of  
21 macrobenthos on cold-water coral mounds and adjacent off-mound habitat in the  
22 bathyal Porcupine Seabight, NE Atlantic, *Deep Sea Res. Part I Oceanogr. Res.*  
23 *Pap.*, 54(4), 654–672, doi:10.1016/j.dsr.2007.01.005, 2007.

24 Holcomb, M., Venn, a a, Tambutté, E., Tambutté, S., Allemand, D., Trotter, J. and  
25 McCulloch, M.: Coral calcifying fluid pH dictates response to ocean acidification.,  
26 *Sci. Rep.*, 4, 5207, doi:10.1038/srep05207, 2014.

27 Hönisch, B., Hemming, S., Grottoli, A.G., Amat, A., Hanson, G.N., Bijma, J.,  
28 2004. Assessing scleractinian corals as recorders for paleo-pH: Empirical  
29 calibration and vital effects. *Geochimica et Cosmochimica Acta* 68, 3675–3685.

30 Janiszewska, K., Stolarski, J., Benzerara, K., Meibom, A., Mazur, M., Kitahara, M.  
31 V and Cairns, S. D.: A unique skeletal microstructure of the deep-sea micrabaciid  
32 scleractinian corals., *J. Morphol.*, 272(2), 191–203, doi:10.1002/jmor.10906,  
33 2011.

34 Juillet-Leclerc, A., Reynaud, S., Rollion-Bard, C., Cuif, J.-P., Dauphin, Y., Blamart,  
35 D., Ferrier-Pagès, C. and Allemand, D.: Oxygen isotopic signature of the skeletal  
36 microstructures in cultured corals: Identification of vital effects, *Geochemica*  
37 *Cosmochem. Acta*, 73, 5320–5332, doi:10.1016/j.gca.2009.05.068, 2009.

1 Kasemann, S. a., Schmidt, D. N., Bijma, J. and Foster, G. L.: In situ boron  
2 isotope analysis in marine carbonates and its application for foraminifera and  
3 palaeo-pH, *Chem. Geol.*, 260(1-2), 138–147,  
4 doi:10.1016/j.chemgeo.2008.12.015, 2009.

5 Klochko, K., Kaufman, A. J., Yao, W., Byrne, R. H. and Tossell, J. a.:  
6 Experimental measurement of boron isotope fractionation in seawater, *Earth  
7 Planet. Sci. Lett.*, 248(1-2), 276–285, doi:10.1016/j.epsl.2006.05.034, 2006.

8 Krief et al Krief, S., Hendy, E.J., Fine, M., Yam, R., Meibom, A., Foster, G.L.,  
9 Shemesh, A., 2010. Physiological and isotopic responses of scleractinian corals to  
10 ocean acidification. *Geochimica Et Cosmochimica Acta* 74, 4988-5001.

11 Lavigne, H. and Gattuso, J.: seacarb: seawater carbonate chemistry with R,  
12 2010.

13 Maier, C., Bils, F., Weinbauer, M. G., Watremez, P., Peck, M. a. and Gattuso, J.-  
14 P.: Respiration of Mediterranean cold-water corals is not affected by ocean  
15 acidification as projected for the end of the century, *Biogeosciences*, 10(8),  
16 5671–5680, doi:10.5194/bg-10-5671-2013, 2013.

17 Maier, C., Hegeman, J., Weinbauer, M. G. and Burg, D.: Calcification of the cold-  
18 water coral *Lophelia pertusa* under ambient and reduced pH, , 1, 1671–1680,  
19 2009.

20 Maier, C., Watremez, P., Taviani, M., Weinbauer, M. G. and Gattuso, J. P.:  
21 Calcification rates and the effect of ocean acidification on Mediterranean cold-  
22 water corals., *Proc. Biol. Sci.*, 279(1734), 1716–23, doi:10.1098/rspb.2011.1763,  
23 2012.

24 McCulloch, M., Trotter, J., Montagna, P., Falter, J., Dunbar, R., Freiwald, A.,  
25 Försterra, G., López Correa, M., Maier, C., Rüggeberg, A. and Taviani, M.:  
26 Resilience of cold-water scleractinian corals to ocean acidification: Boron isotopic  
27 systematics of pH and saturation state up-regulation, *Geochim. Cosmochim. Acta*,  
28 87, 21–34, doi:10.1016/j.gca.2012.03.027, 2012.

29 Melbourne, L.A., Griffin, J., Schmidt, D.N., Rayfield, E.J., 2015. Potential and  
30 limitations of finite element modelling in assessing structural integrity of coralline  
31 algae under future global change. *Biogeosciences Discussions* 12, 3855-3877.  
32 Accepted in *Biogeosciences*

33 Mienis, F., De Stigter, H. C., White, M., Duineveld, G., De Haas, H. and Van  
34 Weering, T. C. E.: Hydrodynamic controls on cold-water coral growth and  
35 carbonate-mound development at the SW and SE Rockall Trough Margin, NE  
36 Atlantic Ocean, *Deep Sea Res. Part I Oceanogr. Res. Pap.*, 54(9), 1655–1674,  
37 2007.

1 Mortensen, P. B. and Rapp, H. T.: Oxygen and carbon isotope ratios related to  
2 growth line patterns in skeletons of *Lophelia pertusa* (L) (Anthozoa, Scleractinia):  
3 Implications for determination of linear extension rates, *Sarsia*, 83, 433–446,  
4 1998.

5 Moya, a, Huisman, L., Ball, E. E., Hayward, D. C., Grasso, L. C., Chua, C. M.,  
6 Woo, H. N., Gattuso, J.-P., Forêt, S. and Miller, D. J.: Whole transcriptome  
7 analysis of the coral *Acropora millepora* reveals complex responses to CO<sub>2</sub>-driven  
8 acidification during the initiation of calcification., *Mol. Ecol.*, 21(10), 2440–54,  
9 doi:10.1111/j.1365-294X.2012.05554.x, 2012.

10 Orr, J. C., Fabry, V. J., Aumont, O., Bopp, L., Doney, S. C., Feely, R. a,  
11 Gnanadesikan, A., Gruber, N., Ishida, A., Joos, F., Key, R. M., Lindsay, K., Maier-  
12 Reimer, E., Matear, R., Monfray, P., Mouchet, A., Najjar, R. G., Plattner, G.-K.,  
13 Rodgers, K. B., Sabine, C. L., Sarmiento, J. L., Schlitzer, R., Slater, R. D.,  
14 Totterdell, I. J., Weirig, M.-F., Yamanaka, Y. and Yool, A.: Anthropogenic ocean  
15 acidification over the twenty-first century and its impact on calcifying organisms.,  
16 *Nature*, 437(7059), 681–6, doi:10.1038/nature04095, 2005.

17 Pörtner, H.O., Karl, D., Boyd, P.W., Cheung, W., Lluch-Cota, S.E., Nojiri, Y.,  
18 Schmidt, D.N., Zavialov, P., 2014. Ocean systems, in: Field, C.B., Barros, V.R.,  
19 Dokken, D.J., Mach, K.J., Mastrandrea, M.D., Bilir, T.E., Chatterjee, M., Ebi, K.L.,  
20 Estrada, Y.O., Genova, R.C., Girma, B., Kissel, E.S., Levy, A.N., MacCracken, S.,  
21 Mastrandrea, P.R., White, L.L. (Eds.), IPCC WGII. Cambridge University Press,  
22 Cambridge, United Kingdom and New York, NY, USA, pp. 411-484.

23 Rae, J.W.B., Foster, G.L., Schmidt, D.N., Elliott, T., 2011. Boron isotopes and  
24 B/Ca in benthic foraminifera: Proxies for the deep ocean carbonate system. *Earth*  
25 *and Planetary Science Letters* 302, 403-413.

26 Ragazzola, F., Foster, L. C., Form, A., Anderson, P. S. L., Hansteen, T. H. and  
27 Fietzke, J.: Ocean acidification weakens the structural integrity of coralline algae,  
28 *Glob. Chang. Biol.*, 18(9), 2804–2812, doi:10.1111/j.1365-2486.2012.02756.x,  
29 2012.

30 Ries, J. B.: A physicochemical framework for interpreting the biological  
31 calcification response to CO<sub>2</sub>-induced ocean acidification, *Geochim. Cosmochim.*  
32 *Acta*, 75(14), 4053–4064, doi:10.1016/j.gca.2011.04.025, 2011.

33 Ries, J. B., Cohen, a. L. and McCorkle, D. C.: Marine calcifiers exhibit mixed  
34 responses to CO<sub>2</sub>-induced ocean acidification, *Geology*, 37(12), 1131–1134,  
35 doi:10.1130/G30210A.1, 2009.

36 Roberts, M., Henry, L.-A., Long, D. and Hartley, J. P.: Cold-water coral reef  
37 frameworks and enhanced megafaunal diversity on the Hatton Bank, NE Atlantic,  
38 *Facies*, 54, 1297–316, 2008.

1 Rodolfo-Metalpa, R., Montagna, P. and Aliani, S.: Calcification is not the Achilles '  
2 heel of cold-water corals in an acidifying ocean, , 2, 2238–2248,  
3 doi:10.1111/gcb.12867, 2015.

4 Rollion-Bard, C., Blamart, D., Cuif, J.-P. and Dauphin, Y.: *In situ* measurements  
5 of oxygen isotopic composition in deep-sea coral , *Lophelia pertusa*: Re-  
6 examination of the current geochemical models of biomineralization, *Geochim.*  
7 *Cosmochim. Acta*, 74(4), 1338–1349, doi:10.1016/j.gca.2009.11.011, 2010.

8 Rollion-Bard, C., Blamart, D., Trebosc, J., Tricot, G., Mussi, A. and Cuif, J.-P.:  
9 Boron isotopes as pH proxy: A new look at boron speciation in deep-sea corals  
10 using <sup>11</sup>B MAS NMR and EELS, *Geochemica Cosmochem. Acta*, 75, 1003–1012,  
11 doi:10.1016/j.gca.2010.11.023, 2011.

12 Schoepf, V., Grottoli, A. G., Warner, M. E., Cai, W.-J., Melman, T. F., Hoadley, K.  
13 D., Pettay, D. T., Hu, X., Li, Q., Xu, H., Wang, Y., Matsui, Y. and Baumann, J. H.:  
14 Coral energy reserves and calcification in a high-CO<sub>2</sub> world at two temperatures.,  
15 *PLoS One*, 8(10), e75049, doi:10.1371/journal.pone.0075049, 2013.

16 Stampanoni, M., Groso, a., Isenegger, a., Mikuljan, G., Chen, Q., Bertrand, a.,  
17 Henein, S., Betemps, R., Frommherz, U., Böhler, P., Meister, D., Lange, M.,  
18 Abela, R. and Boehler, P.: Trends in synchrotron-based tomographic imaging: the  
19 SLS experience, *Dev. X-Ray Tomogr. V*, 6318, 63180M–63180M–14,  
20 doi:10.1117/12.679497, 2006.

21 Stolarski, J.: Three – dimensional micro – and nanostructural characteristics of  
22 the scleractinian coral skeleton: A biocalcification proxy, *Acta Palaeontol. Pol.*,  
23 48(4), 497–530, 2003.

24 Thomsen, J., Casties, I., Pansch, C., Körtzinger, A. and Melzner, F.: Food  
25 availability outweighs ocean acidification effects in juvenile *Mytilus edulis*:  
26 laboratory and field experiments., *Glob. Chang. Biol.*, 19(4), 1017–27,  
27 doi:10.1111/gcb.12109, 2013.

28 Trotter, J., Montagna, P., McCulloch, M., Silenzi, S., Reynaud, S., Mortimer, G.,  
29 Martin, S., Ferrier-Pagès, C., Gattuso, J.-P. and Rodolfo-Metalpa, R.: Quantifying  
30 the pH “vital effect” in the temperate zooxanthellate coral *Cladocora caespitosa*:  
31 Validation of the boron seawater pH proxy, *Earth Planet. Sci. Lett.*, 303(3-4),  
32 163–173, doi:10.1016/j.epsl.2011.01.030, 2011.

33 Venn, A. A., Tambutté, E., Holcomb, M., Laurent, J., Allemand, D. and Tambutté,  
34 S.: Impact of seawater acidification on pH at the tissue – skeleton interface and  
35 calcification in reef corals, *Proc. Natl. Acad. Sci. U. S. A.*, 110(5), 1634–1639,  
36 doi:10.1073/pnas.1216153110, 2013.

37 Wainright, S. A.: Studies of the mineral phase of coral skeleton, *Exp. Cell Res.*,  
38 34, 213–230, 1964.

1 Wall, M. and Nehrke, G.: Reconstructing skeletal fiber arrangement and growth  
2 mode in the coral *Porites lutea* (Cnidaria, Scleractinia): a confocal Raman  
3 microscopy study, *Biogeosciences*, 9(11), 4885–4895, doi:10.5194/bg-9-4885-  
4 2012, 2012.

5

6

7

1 **Table 1:** Summarized environmental and culturing conditions from Form & Riebesell  
 2 (2012) applicable to the specimens and skeletal regions analysed for skeletal boron  
 3 isotopic composition.

4

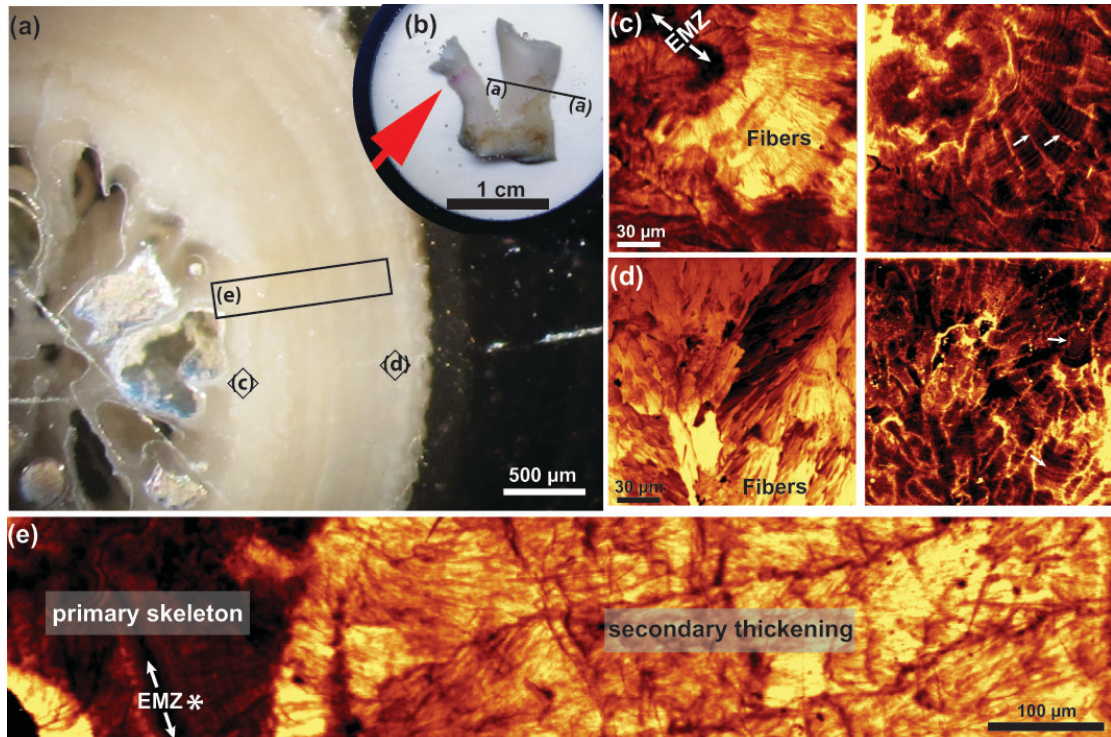
	Sula reef	Cultured CRSIII
Temperature (°C)	7.5	7.5±0.1
Salinity (PSU)	35.2	34.5±0.5
Depth (m)	285	n/a
Total alkalinity (µmol/kg)	2313.7	2349.9 ± 79.5
DIC (µmol/kg)	2149.8	2300.1 ± 89.2
pH <sub>ext</sub> (in total scale)	8.02	7.72 ± 0.056
pCO <sub>2</sub> (µatm)	405	982 ± 146
HCO <sub>3</sub> <sup>-</sup>	2009.3	2192.3 ± 87.0
Ω <sub>Ar</sub>	1.74	0.932 ± 0.097

5

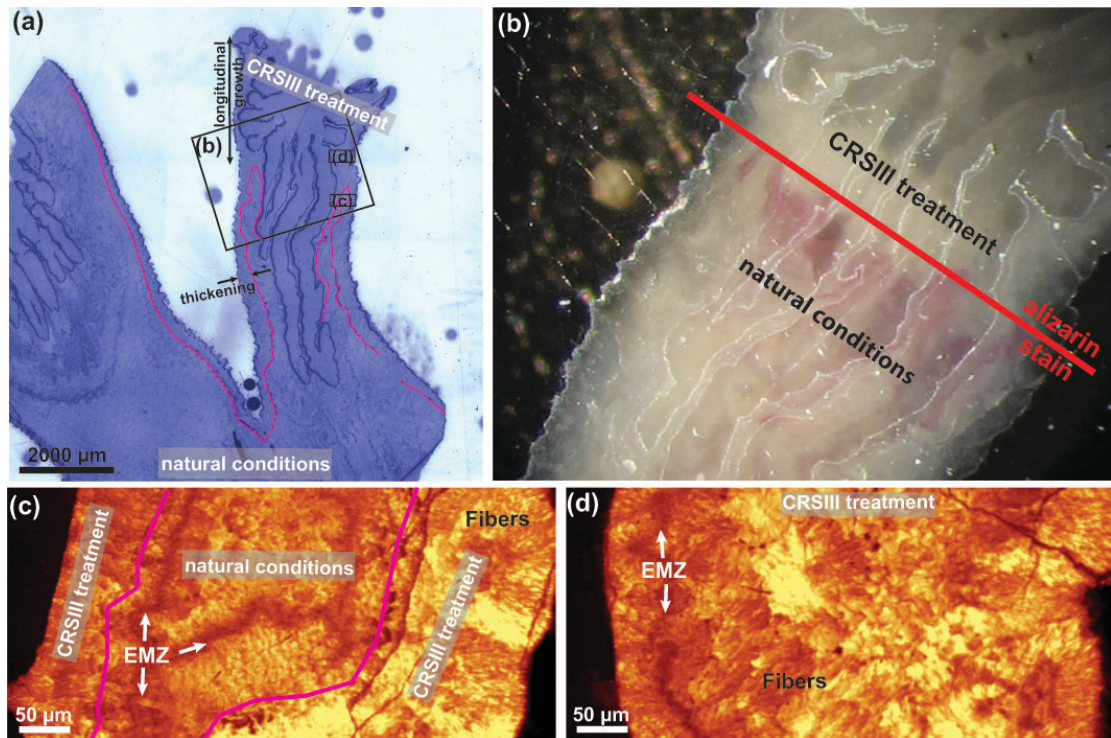
6 **Table 2:** Summary of skeletal boron isotopic composition ( $\delta^{11}\text{B}$ ; mean, standard  
 7 deviation (SD) and standard error (SE)) for different transects on transversal sections  
 8 of different *Lophelia pertusa* polyps (from 3 different colonies) and the corresponding  
 9 pH (mean, min and max). Repeated parallel transects were performed on a few  
 10 polyps. The transect cross different skeletal regions (see Fig. 4-6 and supplementary  
 11 material) here indicated as natural *in situ* grown skeleton (Nat) and/or skeleton grown  
 12 during laboratory culturing conditions (CRSIII).

				$\delta^{11}\text{B}$ transect			pH		
Colony	ind.		skeletal region	mean	SD	SE	min	mean	max
	polyp	Transect							
I	1	1	Nat	<b>26.41</b>	4.09	0.83	8.80	<b>8.85</b>	8.90
I	1	2	Nat	<b>26.08</b>	3.38	0.61	8.79	<b>8.83</b>	8.87
II	2	3	Nat	<b>27.96</b>	2.56	0.48	8.92	<b>8.95</b>	8.98
II	3	4	Nat	<b>27.62</b>	5.10	1.09	8.86	<b>8.93</b>	9.00
II	3	5	Nat	<b>27.55</b>	2.55	0.57	8.89	<b>8.92</b>	8.96
III	4	6	CRSIII	<b>24.81</b>	1.40	0.29	8.76	<b>8.78</b>	8.80
III	4	7	CRSIII	<b>24.74</b>	1.57	0.31	8.75	<b>8.77</b>	8.79
III	4	8	Nat & CRSIII	<b>23.70</b>	2.02	0.41	8.65	<b>8.68</b>	8.70
III	5	9	Nat & CRSIII	<b>25.44</b>	2.75	0.54	8.75	<b>8.79</b>	8.82

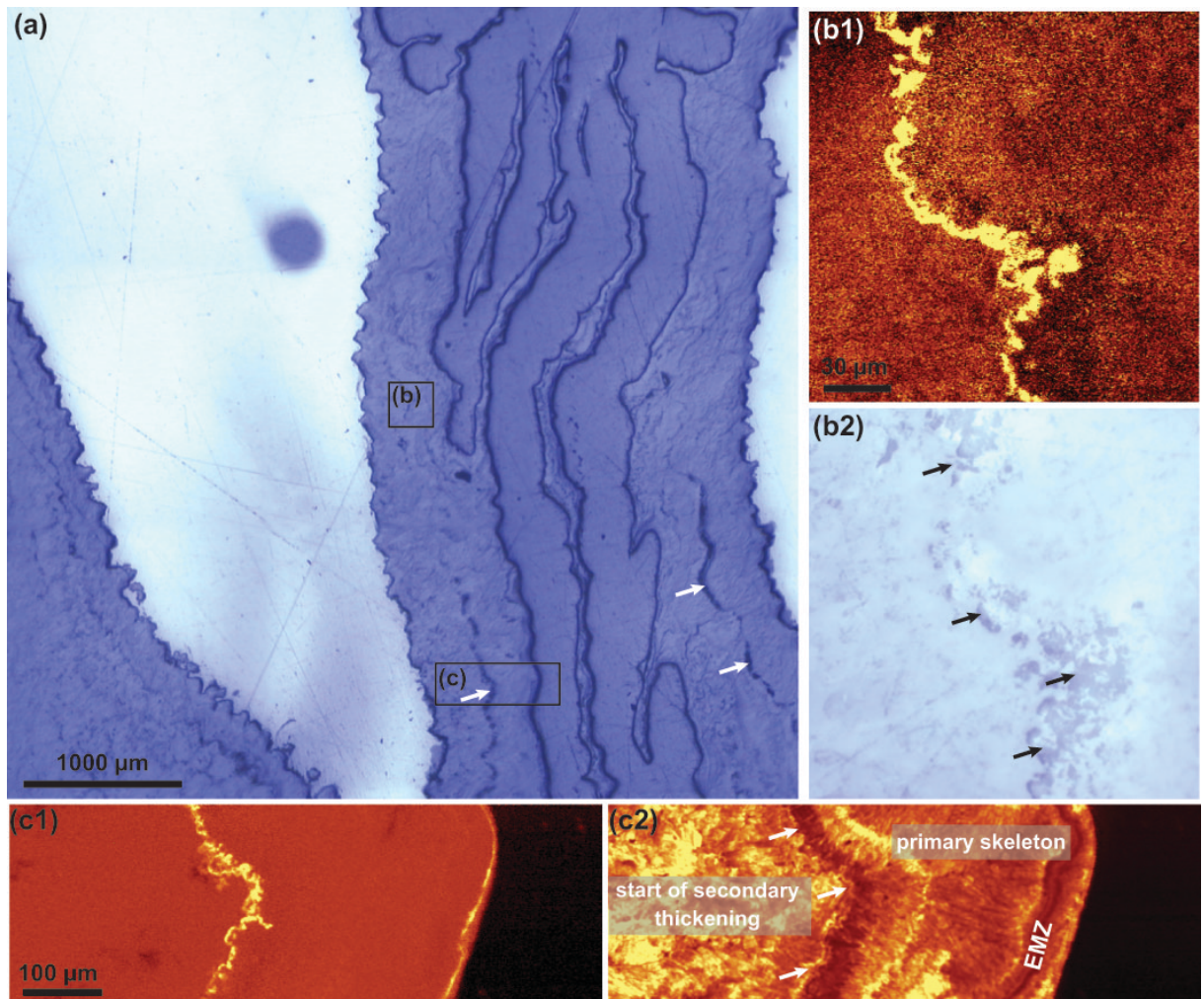
13



1  
 2 **Figure 1:** *Lophelia pertusa* colony (a) cut in transversal plane of an old branch and (b) *Lophelia* colony  
 3 cut in longitudinal plane with two branches (old and a young branch). The young side branch shows  
 4 the Alizarin stain. (c,d) Raman maps of aragonite fibre orientation (left map) and fluorescence (right  
 5 map) within the primary skeleton with early mineralization zone (EMZ; c) and within the secondary  
 6 thickening (d). The arrows in (c,d) mark skeletal organic matrix bands. (e) Raman maps of aragonite  
 7 fibre orientation clearly differentiating primary skeleton and secondary thickening of the corallite and  
 8 early mineralization zone (EMZ).  
 9

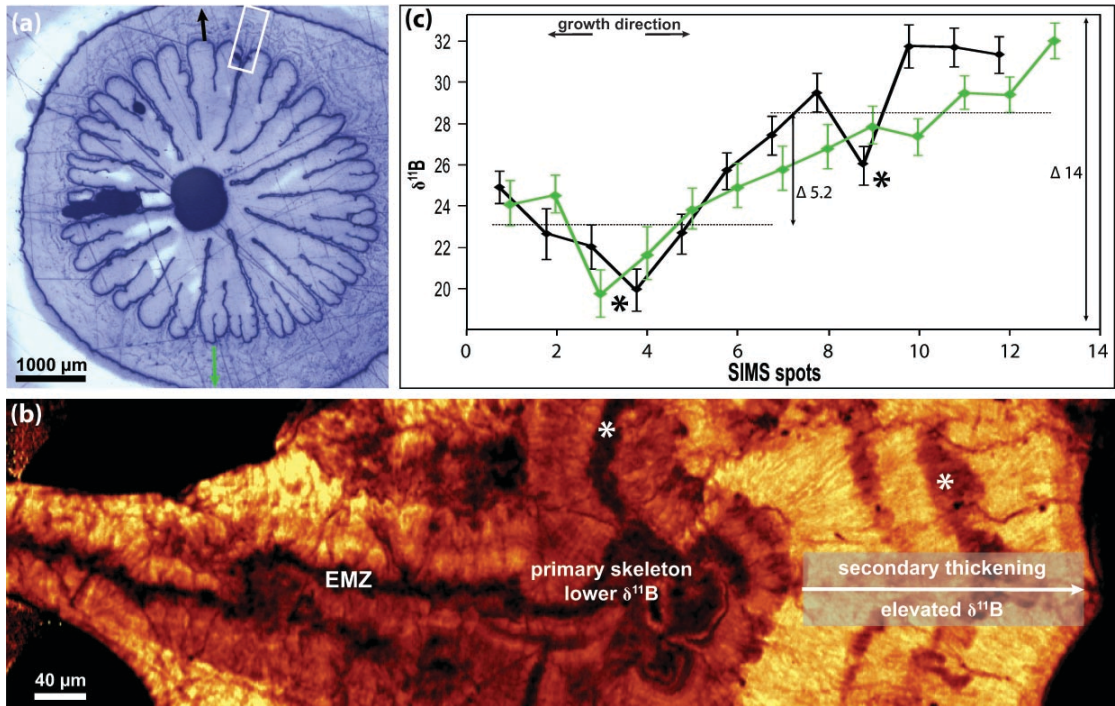


1  
 2 **Figure 2:** (a) *Lophelia pertusa* cut in longitudinal plane through an old and younger colony branch.  
 3 Pink line outlines the position of the staining lines and separates the skeleton grown under natural  
 4 and high CO<sub>2</sub> treatment conditions (CRSIII pCO<sub>2</sub> = 982). (b) Close-up of side branch and location of the  
 5 staining edge above all skeleton was formed during treatment conditions. c,d) Raman map of the  
 6 intensity distribution of the main aragonite peak (symmetric stretch, 1085 cm<sup>-1</sup>) reveals the early  
 7 mineralization zone (EMZ), the primary skeleton and the area of secondary thickening precipitated for  
 8 both natural and treatment conditions.  
 9

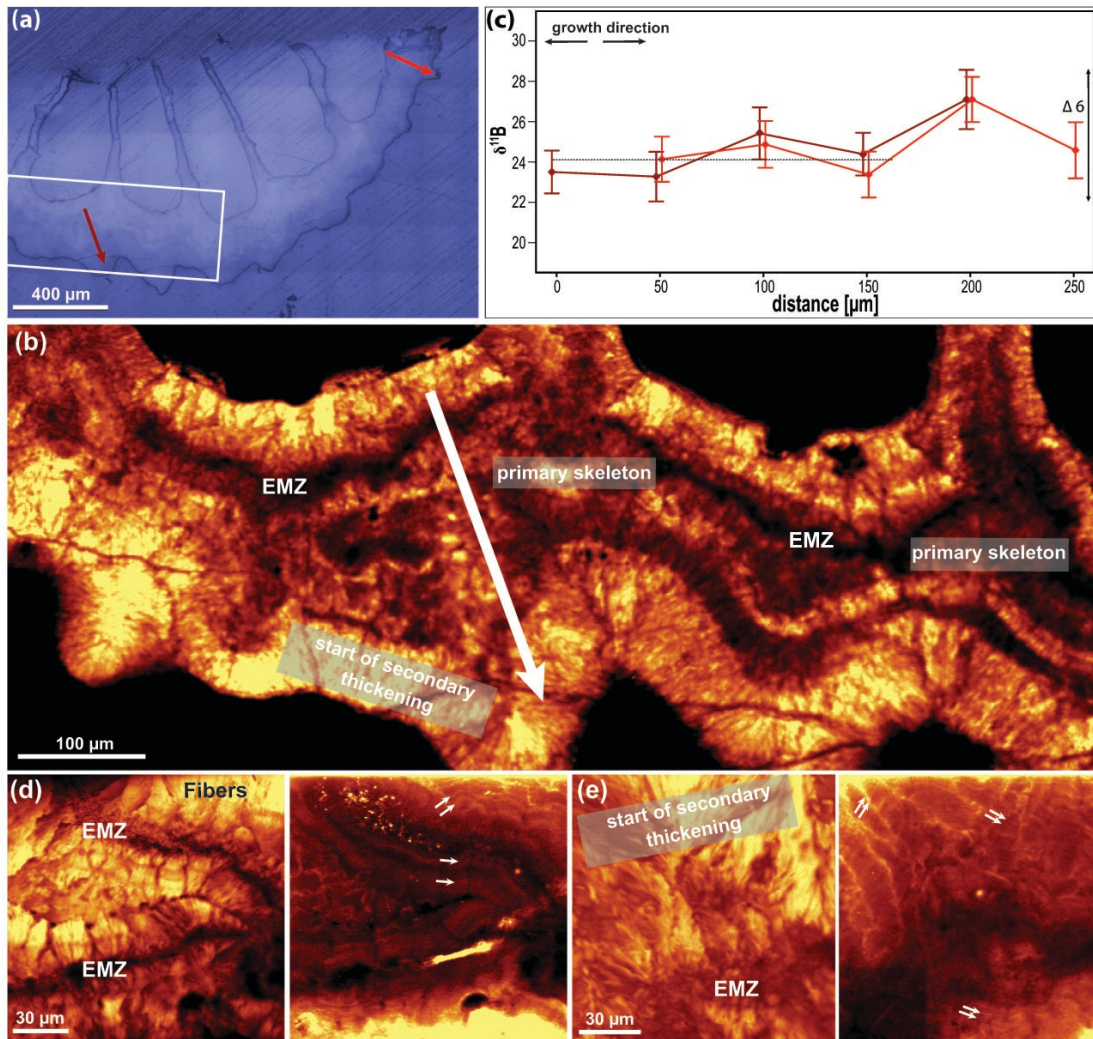


1  
2  
3  
4  
5  
6

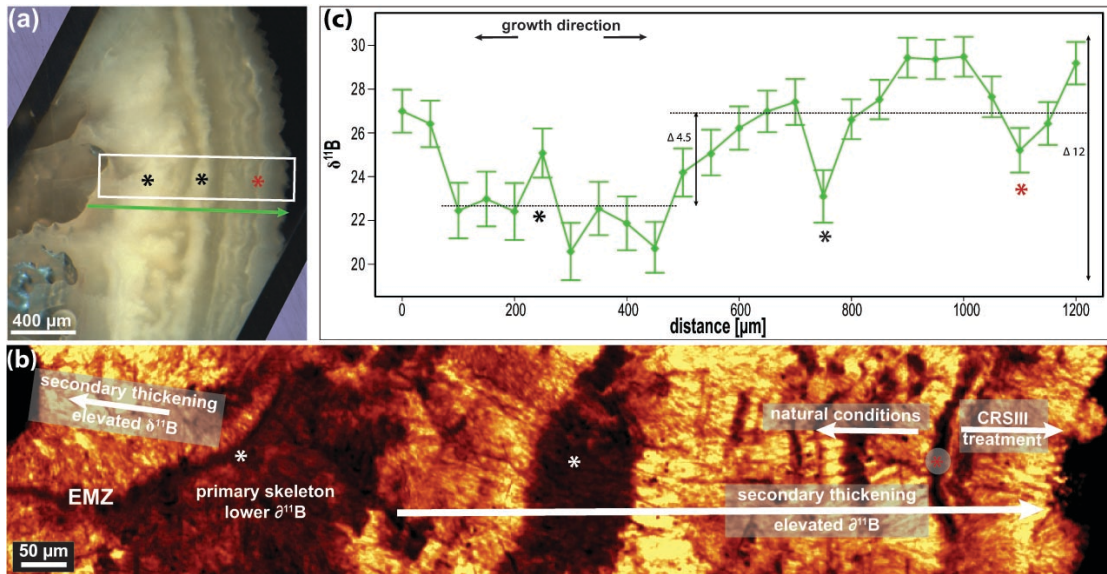
**Figure 3:** (a) *Lophelia pertusa* cut in longitudinal plane displays the location of Raman maps and microscopic image (50x). (b) Raman map of the staining line (b1) and the growth interruptions (black arrows) shown in the microscopic image (b2). (c) Raman maps of the location of the staining line (c1) and the growth interruption seen in aragonite orientation map (c2).



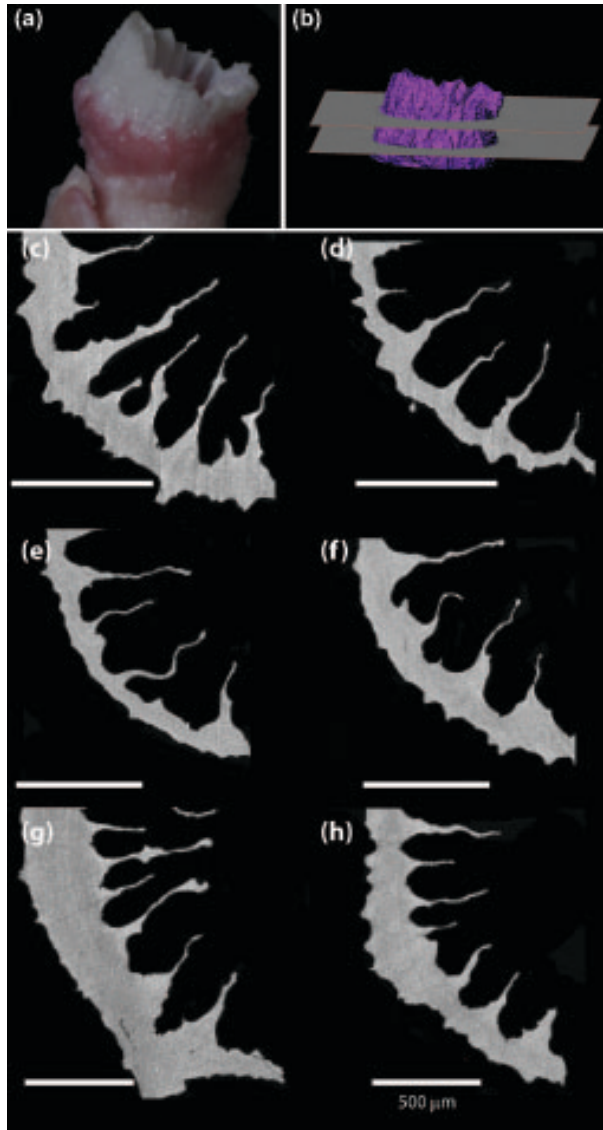
1  
 2 Figure 4: Side branch of *Lophelia pertusa* cut in transversal plane and prepared for Raman mapping  
 3 and SIMS analysis. a) Microscopic image contains the location of the Raman map and the SIMS  
 4 transects. b) Raman map of the intensity distribution of the main aragonite peak (symmetric stretch,  
 5 1085 cm<sup>-1</sup>) reveals the early mineralization zone (EMZ), the primary skeleton and the area of  
 6 secondary thickening. Asterisks mark EMZ in the primary skeleton and skeletal areas within the  
 7 secondary thickening zone of potentially reduced Boron isotopic value (cf. opaque growth bands in  
 8 Blamart et al., 2007 or 1°, 2° nucleation zone in Cohen et al., 2006). c) δ<sup>11</sup>B measured from inside to  
 9 the outer coral skeletal rims (transect #1,2).



1  
2 Figure 5: New branch of *Lophelia pertusa* cut above the staining line in transversal plane and prepared  
3 for Raman mapping and SIMS analysis. a) Microscopic image displays the location of the Raman map  
4 and the SIMS transects. b) Raman map of the intensity distribution of the main aragonite peak  
5 (symmetric stretch,  $1085\text{ cm}^{-1}$ ) reveals the early mineralization zone (EMZ), the primary skeleton and  
6 the start of secondary thickening. c)  $\delta^{11}\text{B}$  measured from inside to the outer coral skeletal rim  
7 (transect #6,7). (d,e) Raman maps of aragonite fibre orientation (left map) and fluorescence (right  
8 map) within the primary skeleton with early mineralization zone (EMZ) and with starting of the  
9 secondary thickening (e). The arrows in (d,e) mark skeletal organic matrix bands.  
10



1  
2 Figure 6: Old branch of *Lophelia pertusa* cut in transversal plane and prepared for Raman mapping  
3 and SIMS analysis. a) Microscopic image of transversal cut through an old branch displaying the  
4 location of the Raman map and SIMS transect. b) Raman map of the intensity distribution of the main  
5 aragonite peak (symmetric stretch,  $1085\text{ cm}^{-1}$ ) reveals the early mineralization zone (EMZ), the  
6 primary skeleton and the area of secondary thickening. Asterisks mark EMZ in the primary skeleton  
7 and skeletal areas within the secondary thickening zone of potentially reduced Boron isotopic value  
8 (cf. opaque growth bands in Blamart et al., 2007 or  $1^\circ$ ,  $2^\circ$  nucleation zone in Cohen et al., 2006)). Red  
9 asterisk marks the location of the staining line and hence, the border between growth under  
10 natural/control condition and laboratory treatment. c)  $\delta^{11}\text{B}$  measured in growth direction from inside  
11 to the outer coral skeletal rim (transect #9).



1  
2  
3  
4  
5  
6

**Figure 7:** (a) Polyp with Alizarin stain and (b) reconstructed SRXTM 3D virtual model. This comparison allowed the virtual polyp to be sectioned below (left panel) and above (right panel) the Alizarin stain. Virtual SXRTM cross-sections of polyps for different pCO<sub>2</sub> treatment 604 μatm (c,d), 778 μatm (e,f) and 982 μatm (g,h).